An Examination of the Ternary Methane + Carbon Dioxide + Water Phase Diagram using the SAFT-VR Approach

J. M. Míguez,[†] M. C. dos Ramos,[‡] M.M. Piñeiro,[†] and F. J. Blas[*,¶]

Departamento de Física Aplicada, Universidade de Vigo, E36310, Vigo, Spain, Department of Chemical and Biomolecular Engineering Department, Vanderbilt University, Nashville, TN 37235 USA , and Departamento de Física Aplicada, Universidad de Huelva, E21071, Huelva, Spain

E-mail: felipe@uhu.es

Phone: +34 959019796. Fax: +34 959219777

---

[*] To whom correspondence should be addressed

[†] Departamento de Física Aplicada, Universidade de Vigo, E36310, Vigo, Spain

[‡] Department of Chemical and Biomolecular Engineering Department, Vanderbilt University, Nashville, TN 37235 USA

[¶] Departamento de Física Aplicada, Universidad de Huelva, E21071, Huelva, Spain

Abstract

In this work, the molecular based Variable Range Statistical Associating Fluid Theory (SAFT-VR) has been used to estimate the global phase equilibria diagram of the ternary mixture water + carbon dioxide + methane, over a wide pressure and temperature range. An accurate determination of the phase equilibria of this mixture is relevant in Petrophysics, as for instance in enhanced natural gas recovery from low permeability reservoirs (the so called tight gas reservoirs), or in geology, as it is the basic composition of many geological fluids. A previous study on the phase behaviour of the binary mixtures involved is presented, using in a transferable manner the characteristic molecular parameters for the three molecules involved. The ternary mixture presents a very rich and complex phase behaviour, with a wide region of the thermodynamic space of phases (at higher pressures) presenting a large gap of ternary liquid−liquid equilibria, that upon descending on pressures leads to the transition to a three phase liquid− liquid−vapour equilibria region, and both regions are separated by a continuous critical endpoint line. The ability of the theory to describe this complex multicomponent mixture phase transition with a reduced and physically sound set of characteristic parameters must be underlined.

Introduction

Natural gas extraction from the so-called non conventional sources is gaining a remarkable relevance due to the increasing global demand of gas supply. These alternative sources include gas hydrates, coalbed methane, shale gas, and the tight-gas reservoirs (TGRs).[1,2] TGRs are low permeability reservoirs, where the usual extraction techniques produce low gas yields. The global amount of natural gas that has been located trapped in this type of reservoirs undoubtedly points to TGRs as one of the main natural gas sources in the near future. Nevertheless, the optimal fracturation and extraction method for these reservoirs has not been determined yet, and it constitutes a challenging topic in Petrophysics. One of the key points in the extraction process commonly employed is the injection of an external aqueous based fluid, with the aim to modify the natural gas adsorption on the solid substrate, enhancing fluid recovery. Apart from the macroscopic engineering concerns, the interfacial phenomena occurring at molecular level in this scenario are poorly understood despite their important role in the process. Interfacial properties and fluid-substrate interaction at this scale determine the behaviour of the transport properties of the fluid, and contributions in this field are essential in order to gain insight into the involved phenomena. In particular, the modification of the original fluid-substrate reservoir conditions after the injection of the external fluid needs to be precisely described.

But before considering the effects induced by the presence of a solid substrate on a fluid mixture, it is essential to have, as starting reference, an accurate quantitative description of its global phase equilibria in bulk conditions, at temperature and pressure ranges close to those that are presumed to be found in real reservoirs. This picture of the bulk system phase equilibria scheme is an essential information to guess which among the possible interfacial scenarios are bound to occur, and how the concentration, for instance, will modify the mixture behaviour to improve extraction conditions. Thus, the preliminary study of thermodynamic properties for bulk multicomponent mixtures that include methane, water, and other polar compounds plays a central role in this context. As an example, the importance of the water + methane binary mixture in the characterization of aqueous fluid inclusions in petroleum basins may be cited.[3] Carbon dioxide is a molecule that may be considered as well in the composition of these geochemically relevant mixtures, because its geologic sequestration is envisaged as a potential derived benefit of the extraction processes. In fact, a combination of carbon dioxide and water is already pumped into depleted oil wells to repressurize them and enhance oil recovery. Another application involving carbon dioxide, water and methane is the injection of CO_2 into deep sea methane hydrate reservoirs, with the double objective of releasing methane and capturing carbon dioxide in the hydrate structure.[4] Due to the complexity of the phase behaviour that may occur when considering multicomponent fluid mixtures, the selection of a physically sound and versatile theoretical model, with demonstrated predictive ability for the estimation of complex phase equilibria diagrams plays a central role in the process.

In this paper, the objective is to estimate the ternary phase equilibria diagram of the water +

carbon dioxide+ methane mixture, over the whole composition range, and in pressure and temperature ranges close to those that are supposed to exist in TGRs. The model used for this study is the Variable Range Statistical Associating Fluid molecular equation of state (SAFT-VR EoS[5,6]).

In previous works,[7,8] the same approach has been used to accurately determine the water + carbon dioxide binary mixture phase diagram, using the intermolecular interaction parameters determined by Galindo and Blas[9,10] and Clark *et al.*[11] This binary mixture exhibits type III phase behaviour, according to the classification of Scott and van Konynenburg,[12,13] and due to its practical relevance, a large number of papers has been devoted to determine experimentally their phase equilibria, with special focus on the mutual solubilities. It is beyond the scope of this paper to present an exhaustive review of experimental data, but the paper of Spycher *et al.*[14] may be cited as an example, because it considers the pressure and temperature ranges of interest involved in carbon dioxide sequestration. Valtz *et al.*[15] determined experimentally vapour liquid equilibria for this binary, using SAFT-VR EoS as estimation tool. Other authors have tried different theoretical approaches to estimate the phase equilibria of this mixture. As recent examples, Pappa *et al.*[16] have modelled the VLE of this mixture using a cubic EoS (Peng-Robinson), and Sun and Dubessy[17] considered a SAFT Lennard-Jones EoS version that included additional dipolar and quadrupolar terms to describe the intermolecular interactions. Recently, Lafitte *et al.*[18] used the so called SAFT VR Mie[19] approach to describe the VLE of this mixture, and used this calculation as starting point, coupling it to an inhomogeneous media theory (Gradient Theory) to describe the fluid-fluid interfacial phenomena, including wetting and adsorption, ocurring for this binary mixture. This latter application emphasizes the need of an accurate thermodynamic model describing both phase equilibria and thermophysical properties of the studied mixture, as a tool to further studies concerning, for instance, interfacial phenomena, which play a crucial role for the practical applications envisaged. From another perspective, Kontogeorgis *et al.*[20] have recently used the CPA EoS to analyze the behaviour of this binary, among other associating systems, with the objective to discuss several formulations describing the effect of crossed interactions between molecules and a feasible way to relate characteristic molecular parameters through an homomorph approach.

The binary mixture water + methane exhibits as well type III phase behaviour, as described in the review of the phase equilibria of the series of water + *n*-alkane mixtures presented by Galindo *et al.*,[21] and finally the mixture carbon dioxide + methane presents type I behaviour.[10,22] The references gathered in the cited articles show the extensive experimental and theoretical studies carried out for these three binary mixtures, but the ternary system has received much less attention due to the complexity of its phase diagram, that will be illustrated by the results shown in the present work. The scarce experimental works concerning this ternary mixture phase equilibria[23–25] are mainly focused on solubilities and VLE. Seo and Lee[26] determined experimental phase equilibria considering the presence of solid hydrates. From a modelling perspective, Duan et al.[27] presented an EoS for the ternary mixture based on the virial expansion, for an extended temperature and pressure range, justifying the study on the presence and relevance of this ternary mixture in many geological fluids. Austegard et al.[28] considered also this ternary mixture, focusing on the estimation of mutual solubilities of water in carbon dioxide and water in solutions of methane and carbon dioxide. For these purpose the authors used several cubic EoS approaches, as Soave-Redlich-Kwong[29] with different combining rules and the so-called Cubic Plus Association (CPA[30]) EoS. This paper tests various parametrization schemes and discusses the influence of the combining rules selected on the correlation of the experimental data.

Molecular Model and Theory

In the SAFT-VR approach, molecules are modelled with a simple united atom approach as chains composed of m tangentially bonded segments of equal diameter σ, which interact through a potential of variable range, typically the square-well (SW) potential. The interactions in the SW potential between segments i and j separated by a distance r_{ij} is given by,

$$u_{ij}(r_{ij}) = \begin{cases} +\infty & \text{if } r_{ij} < \sigma_{ij} \\ -\varepsilon_{ij} & \text{if } \sigma_{ij} \leq r_{ij} \leq \lambda_{ij}\sigma_{ij} \\ 0 & \text{if } r_{ij} > \lambda_{ij}\sigma_{ij} \end{cases} \tag{1}$$

where σ_{ij} defines the contact distance between spheres, and λ_{ij} and ε_{ij} are the range and depth of the potential well for the i-j interaction, respectively.

In this work we are considering three types of molecules: water (H_2O), methane (CH_4) and carbon dioxide (CO_2). The model for H_2O molecules is based of the four-site model proposed by Bol[31] and Nezbeda *et al.*,[32] where each molecule is represented as a hard sphere of diameter σ_{11}, with four off-centre short-range attractive sites that mediate the hydrogen-bonding interactions. Two associating sites (of type H) represent the hydrogen atoms in the H_2O molecule and the other two sites (of type O) represent the lone pairs of electrons of the oxygen, where only H−O site-site interactions are allowed, i.e. no H−H or O−O interactions are permitted. The associating sites are located at a distance $r_{d_{11}}$ from the centre of the sphere and have a cut off range of $r_{c_{11}}$, so that when the site-site distance is less than $r_{c_{11}}$ a hydrogen-bonding energy of interaction ε_{11}^{hb} is realised. We use the optimal intermolecular parameters for H_2O previously determined by Clark *et al.*[11] The CH_4 molecule is represented by an spherical segment of hard-sphere diameter σ_{22}, whose intermolecular parameters were determined in the work of Patel *et al.*[33] The third molecule considered here, CO_2, is modelled as two tangentially bonded hard-sphere segments of equal diameter σ_{33}, with molecular parameters obtained from the work of Galindo and Blas.[9,10] It is important to mention that the polar and quadrupolar interactions of H_2O and CO_2 are treated in an effective way via the dispersive interactions. Although, it is worth to mention that CO_2-CO_2 and CO_2-H_2O association interactions have been discussed by previous authors, such as Ji *et al.*,[34] who treated the quadropular moment of CO_2 and H_2O molecules via association, and Valtz *et al.*,[15] who has suggested that the unusual large interaction parameters they found for the $H_2O + CO_2$ mixture is due to the lack of a cross-association scheme. However, Valtz *et al.* realised that when incorporating this kind of unlike interactions the bonding energy values obtained were close to zero and as such they rejected the idea. Therefore, we have considered both CH_4 and CO_2 to be non-associating molecules and thus no unlike association was considered.

We examine the phase equilibria of the $H_2O + CH_4 + CO_2$ ternary system using the SAFT-VR approach. Since this theory has already been presented and used previously,[5,6] here we only give an brief overview of the main expressions. As any other SAFT version, the SAFT-VR approach is written in terms of the Helmholtz free energy, which can be expressed as a sum of four microscopic contributions: an ideal contribution (A^{IDEAL}), a monomer term (A^{MONO}) that takes into account the attractive and repulsive forces between the segments that form the molecules, a chain contribution (A^{CHAIN}) that accounts for the connectivity of segments within the molecules, and an association contribution (A^{ASSOC}) that accounts for the hydrogen bonding interactions between molecules. Then, the Helmholtz free energy is written as,

$$\frac{A}{Nk_{\mathrm{B}}T} = \frac{A^{\mathrm{IDEAL}}}{Nk_{\mathrm{B}}T} + \frac{A^{\mathrm{MONO}}}{Nk_{\mathrm{B}}T} + \frac{A^{\mathrm{CHAIN}}}{Nk_{\mathrm{B}}T} + \frac{A^{\mathrm{ASSOC}}}{Nk_{\mathrm{B}}T} \tag{2}$$

where N is the total number of molecules, T is the temperature, and k_{B} is the Boltzmann constant.

The Helmholtz free energy of an ideal mixture of n components is given by,[35]

$$\frac{A^{\mathrm{IDEAL}}}{Nk_{\mathrm{B}}T} = \sum_{i=1}^{n} x_i \ln \rho_i \Lambda_i^3 - 1 \tag{3}$$

where $\rho_i = \frac{N_i}{V}$ represents the molecular number density of component i, N_i, x_i, and Λ_i are the number of molecules, the molar fraction, and the thermal de Broglie wavelength of species i, respectively; and V is the volume of the system.

The monomer free energy is given by a second-order high-temperature expansion of Barker and Henderson perturbation theory for mixtures,[36–38]

$$\frac{A^{\mathrm{MONO}}}{Nk_{\mathrm{B}}T} = \frac{A^{\mathrm{HS}}}{Nk_{\mathrm{B}}T} + \frac{A_1}{Nk_{\mathrm{B}}T} + \frac{A_2}{Nk_{\mathrm{B}}T} \tag{4}$$

where $\frac{A^{\mathrm{HS}}}{Nk_{\mathrm{B}}T}$ is the free energy of reference hard-sphere mixture, which is obtained from the expression of Boublik[39] (equivalent to that of Mansoori *et al.*[40]); while $\frac{A_1}{Nk_{\mathrm{B}}T}$ and $\frac{A_2}{Nk_{\mathrm{B}}T}$ are the first- and second-order perturbation terms associated with the attractive interactions $u_{ij}(r_{ij})$ given by Eq. (1), where the former is treated in the context of the M1Xb mixing rule[5,6] and the latter is obtained using the local compressibility approximation.

The contribution to the free energy due to chain formation of square-well segments for a mixture of chains is given by,[41]

$$\frac{A^{\mathrm{CHAIN}}}{Nk_{\mathrm{B}}T} = -\sum_{i=1}^{n} x_i \left(m_i - 1\right) \ln y_{ii}^{\mathrm{SW}}(\sigma_{ii}) \tag{5}$$

where m_i is the number of segments of component i, and $y_{ii}^{\mathrm{SW}}(\sigma_{ii})$ is the background correlation function , $y_{ii}^{\mathrm{SW}}(\sigma_{ii}) = g_{ii}^{\mathrm{SW}}(\sigma_{ii}) \exp\left(-\beta\varepsilon_{ii}\right)$, which is given in terms of the contact pair radial distribution function for a mixture of square-well segments corresponding to the $i-i$ interaction. $g_{ii}^{\mathrm{SW}}(\sigma_{ii})$ is obtained from a first-order high-temperature expansion[36–38] (see references[5,6] for further details). Note that in our system, the only chain formation to account for in the free energy is due to the CO_2 chain model molecule, since both H_2O and CH_4 are modelled as spherical segments.

Finally, the contribution to the free energy due to the association of s_i sites on a molecule of species i can be obtained from the theory of Wertheim[42–45] as,

$$\frac{A^{\mathrm{ASSOC}}}{Nk_{\mathrm{B}}T} = \sum_{i=1}^{n} x_i \left[\sum_{a=1}^{s_i} \left(\ln X_{a,i} - \frac{X_{a,i}}{2}\right) + \frac{s_i}{2}\right] \tag{6}$$

where the first sum is over component i and the second over all s_i sites of type a on a molecule i. The fraction $X_{a,i}$ of molecules i not bonded at site a is given by the mass action equation as:[46,47]

$$X_{a,i} = \frac{1}{1 + \rho \sum_{j=1}^{n} x_j \sum_{b=1}^{s_j} X_{b,j} \Delta_{a,b,i,j}} \tag{7}$$

Here, $\Delta_{a,b,i,j}$ characterises the association between site a on molecule i and site b on molecule j and can be written as,

$$\Delta_{a,b,i,j} = K_{a,b,i,j} f_{a,b,i,j} g_{ij}^{\mathrm{SW}}(\sigma_{ij}) \tag{8}$$

where the Mayer f-function of the $a-b$ site-site association interaction ($\phi_{a,b,i,j}$) is given by $f_{a,b,i,j} = \exp(-\frac{\phi_{a,b,i,j}}{\mathrm{k_B}T}) - 1$, and $K_{a,b,i,j}$ is the available volume for bonding, whose expression can be found elsewhere.[5,6,46,47] Since there is only one associating component in the mixture (i.e. the H_2O molecule) that is only allowed to form one type of hydrogen bond (i.e. $H-O$), with no unlike association interactions between H_2O-CO_2 and H_2O-CH_4, the association contribution can be greatly simplified, and the fractions $X_{a,i}$ of H_2O molecules not bonded at any of the four sites are equivalent.

The study of phase equilibria in mixtures also requires the determination of a number of cross interaction parameters, which account for the interactions between unlike components in the mixture. The Lorentz arithmetic mean is used for the unlike hard-core diameter,

$$\sigma_{ij} = \frac{\sigma_{ii} + \sigma_{jj}}{2} \tag{9}$$

and the unlike square-well potential range parameter is given by,

$$\lambda_{ij} = \frac{\lambda_{ii}\sigma_{ii} + \lambda_{jj}\sigma_{jj}}{\sigma_{ii} + \sigma_{jj}} \tag{10}$$

The unlike square-well dispersive energy parameter is given by a modified Berthelot rule as follows,

$$\varepsilon_{ij} = \xi_{ij}\sqrt{\varepsilon_{ii}\varepsilon_{jj}} \tag{11}$$

where ξ_{ij} describes the departure of the system from the geometric mean; it is usually determined by comparison with mixture data and then used to predict properties at different conditions.

Other thermodynamic properties, such as the chemical potential (μ), compressibility factor (Z), and other thermodynamic derivatives needed in our calculations can be easily obtained from the Helmholtz free energy using standard thermodynamic relations.

Results and discussion

The SAFT-VR approach requires the determination of a number of intermolecular parameters to describe the thermodynamic properties of real substances. For the non-associating CH_4 and CO_2

molecules, four parameters are needed to characterise the model, namely the chain length (m_i), the hard-core diameter of the segments (σ_{ii}), the depth (ε_{ii}) and range (λ_{ii}) of the SW potential. In the case of H_2O (associating), apart from the m_1, σ_{11}, ε_{11} and λ_{11} set of parameters, additional parameters are necessary to describe the hydrogen bonding interactions such as the number and type of associating sites, the site-site energy parameter (ε_{11}^{hb}) and the volume available for bonding (K_{11}^{hb}, which is given in terms of $r_{c_{11}}$, $r_{d_{11}}$ and σ_{11}[48]). These parameters are usually obtained by fitting the theory to the experimental values of the vapour pressure and saturated liquid densities. In this work, we use the set of parameters obtained previously in the work of Clark *et al.*[11] for H_2O, Patel *et al.*[33] for CH_4 and work of Galindo and Blas[9,10] for CO_2, as reported in Table 1. This set of parameters has been shown to provide an excellent description of the phase behaviour at a wide range of temperatures, except the area near the critical point. It is known that SAFT, as any other classical equation of state or mean field approach, does not consider the density fluctuations that occur near the critical point and hence the correct physics of the problem is not described and an over-prediction of its coordinates is expected. This can be easily addressed in an effective way by re-scaling the conformal parameters (σ_c and ε_c) to the experimental critical temperature and pressure. The re-scaled parameters are also presented in Table 1. The remaining, non-conformal parameters, are kept fixed in reduced units, but their corresponding values in real units are also presented in the table for clarity. It is obvious that use of the re-scaled parameters produces a detriment in the calculated saturated liquid density of pure components, as it has been shown in previous works.[9–11] However, these sets of parameters provide a good description of the coexistence compositions and critical curves. A more satisfactory description of these systems could be obtained using the new version of SAFT-VR proposed by Forte *et al.*[49] in combination with the renormalization-group theory.

A summary of the results obtained for the three binary mixtures involved will be presented before discussing the phase equilibria diagram obtained for the ternary mixture. As mentioned before, the two binaries containing water exhibit type III phase behaviour. The most representative feature of this type of mixtures is that, in a PT projection of the phase diagram, the gas-liquid

Table 1: Optimised and Rescaled Square-Well Intermolecular Potential Parameters for Water,[11] Methane[33] and Carbon Dioxide[9,10]

Molecule	Water	Methane	CO_2
m	1	1	2
σ (Å)	3.033	3.685	2.786
ε/k_B (K)	300.43	167.30	179.27
λ	1.718	1.448	1.515
ε^{HB}/k_B (K)	1336.9		
K^{HB} (Å^3)	0.89369		
σ_c (Å)	3.470	4.058	3.136
ε_c/k_B (K)	276.24	156.46	168.84
ε_c^{HB}/k_B (K)	1229.273		
K_c^{HB} (Å^3)	1.33791		

critical line is discontinuous and presents two branches. One of them, starting at the critical point of the less volatile compound, moves towards higher pressures with negative slope, goes through a temperature minimum, and then continues with positive slope reaching temperatures higher than the one corresponding to the initial critical point. Due to the occurrence of this temperature minimum, this particular case of type III is also denoted as type IIIm, or alternatively it is referred to as well as type IIIb. The existence of phase equilibria beyond the critical temperature of the heaviest compound is characteristic of this type of systems only, and is commonly referred to as gas-gas inmiscibility of second kind, although the densities of the coexisting phases in the higher pressure and temperature ranges are typically liquid like. The other branch of the gas-liquid critical line starts at the lightest compound critical point, and it is very short, ending at a upper critical end point (UCEP), meeting there a three phase (liquid-liquid-vapour) equilibrium line coming from the low temperature and pressure region. This global behaviour means that there is a continuous transition from liquid-vapour to a wide region of liquid-liquid equilibria for the mixture, which added to the temperature minimum of the high pressure critical line and the three phase line constitutes a remarkably complex scenario representing a demanding challenge for any EoS. This type of phase behaviour is typical of mixtures with a large degree of inmiscibility between the pure compounds.

H_2O + CO_2 binary mixture

For the $H_2O + CO_2$ binary, the calculations performed in this paper repeated the scheme proposed in earlier works,[7,8] so only a brief description wil be presented here. Figure 1 recalls the estimated PT phase diagram, exhibiting the distinctive features described above, and let us just recall that a single binary unlike dispersive energy parameter ($\xi_{12} = 0,9742$), was fitted to improve the description of the experimental temperature minimum of the high temperature branch of the fluid-fluid critical line. This model represents adequately the whole phase diagram, with a satisfactory quantitative agreement with experimental literature data. Figure 1 plots available vapour pressure experimental data for pure water[50–58] and CO_2,[59–64] as well as data on the high pressure branch of the liquid vapour critical line[65,66] and three phase line,[15] showing remarkable quantitative agreement in all cases.

H_2O + CH_4 binary mixture

The $H_2O + CH_4$ mixture behaviour is similar to the previous case, as noted. A comprehensive review of the global phase equilibria of the water + *n*-alkane mixtures series has been presented by Galindo *et al.*[21] For this homologous series, the influence of the strong hydrogen bonding between water molecules is one of the main causes that results in type III behaviour, up to *n*-eicosane. Nevertheless, it is necessary to keep in mind that, strictly speaking, the $H_2O + CH_4$ mixture can not be regarded as the first member of this family, due to the particularities exhibited by CH_4 if compared with other linear alkanes, as for instance its anomalous critical pressure.[67] For this reason, this binary mixture deserves an individual detailed study and parameters obtained from other mixtures of the same family do not yield accurate estimations if they are applied in a transferable manner to this particular solution. In this case, the computed PT phase diagram is presented in Figure 2 . Experimental data[68–71] of the temperature minimum of the high pressure branch of the LV critical line have been plotted also in this figure, showing good agreement with the SAFT estimated curve. The inset of this Figure represents the Tx projection of this branch of the critical line, and this view of the estimated curve shows a shift of the calculated minimum

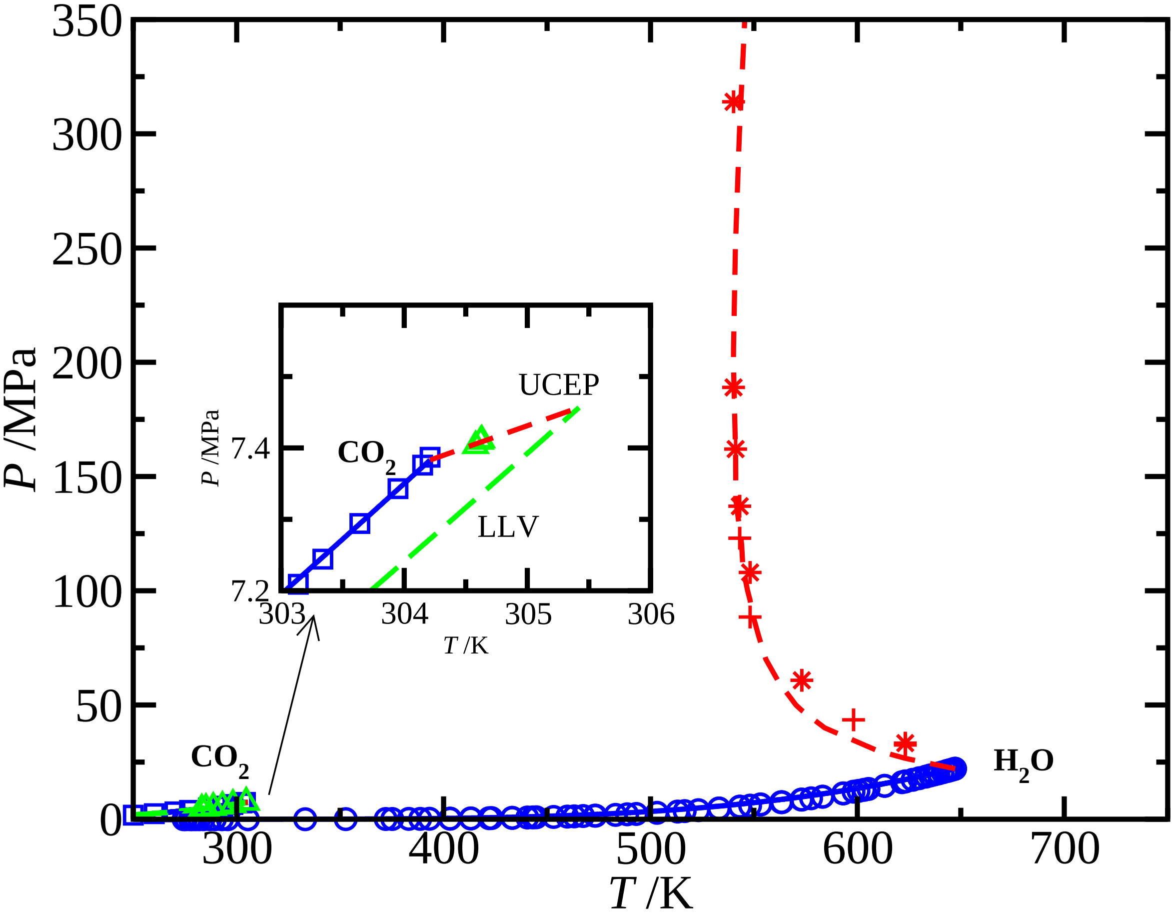

Figure 1: *PT* projection of the phase diagram for the water(1) + carbon dioxide(2) binary mixture. The circles correspond to the experimental vapour pressure data of pure water,[50–58] the squares to the experimental vapour pressure of pure carbon dioxide,[59–64] the stars[65] and pluses[66] to the experimental gas-liquid critical line, and the triangles to the three-phase line.[15] The continuous curves are the SAFT-VR predictions for the vapour-pressures, the dashed curves for the critical lines and the long-dashed curve for the LLV three-phase line. The inset shows the region close to the critical point of pure CO$_2$.

towards higher water content compositions. Despite this displacement, it must be recalled here that for the calculations presented here, no binary mixing rule parameter was determined, and the results shown arise directly from the use of the pure component characteristic parameters listed in Table 1. The reason why in this case this ξ_{12} parameter is not necessary may be connected with the fact that methane is a non polar molecule, so the representation of the molecule as a single sphere interacting through a square well potential is rather realistic, while on the other hand the use of two tangent spheres for carbon dioxide appears not to suffice, as its quadrupolar nature is not explicitly accounted for, and this entails the need of a correcting factor to improve the representation of the mixture behaviour. In this case, the magnification of the region close to the CH_4 critical point has not been shown as an inset in the Figure, as we did in the case of the precedent binary mixture, because the LLV three pase line is virtually superposed to the pure compound saturation curve, so this representation would be worthless here.

Figure 3a shows Px projections of the phase diagram, at temperatures ranging from 350 to 550 K, together with the experimental data of Fletcher *et al.*[73] This range of temperatures lies above the UCEP, so no three phase equilibria appears, and below the temperature minimum of the high temperature branch of the liquid vapour critical line. The trend shown in this case by the coexistence envelope is the typical III phase equilibrium type transition from vapour liquid equilibrium at low pressures to liquid liquid equilibrium at high pressures. Figure 3b plots Tx projections of the phase diagram at pressures ranging from 5 to 100 MPa, showing the estimated high pressure liquid liquid equilibria of the system, together with the corresponding experimental points of the LV critical line for the higher pressures of this calculation (30, 50 and 100 MPa). The correspondence between these experimental points and the estimated high pressure LL coexistence curves is very good, and it must be taken into account that the range of pressures here is very far from the one where the pure compound experimental data used for characteristic parameter fitting were placed, ensuring a remarkable extrapolation ability for the theory over wide ranges of temperature and pressure, which is essential for the practical application that justifies this analysis.

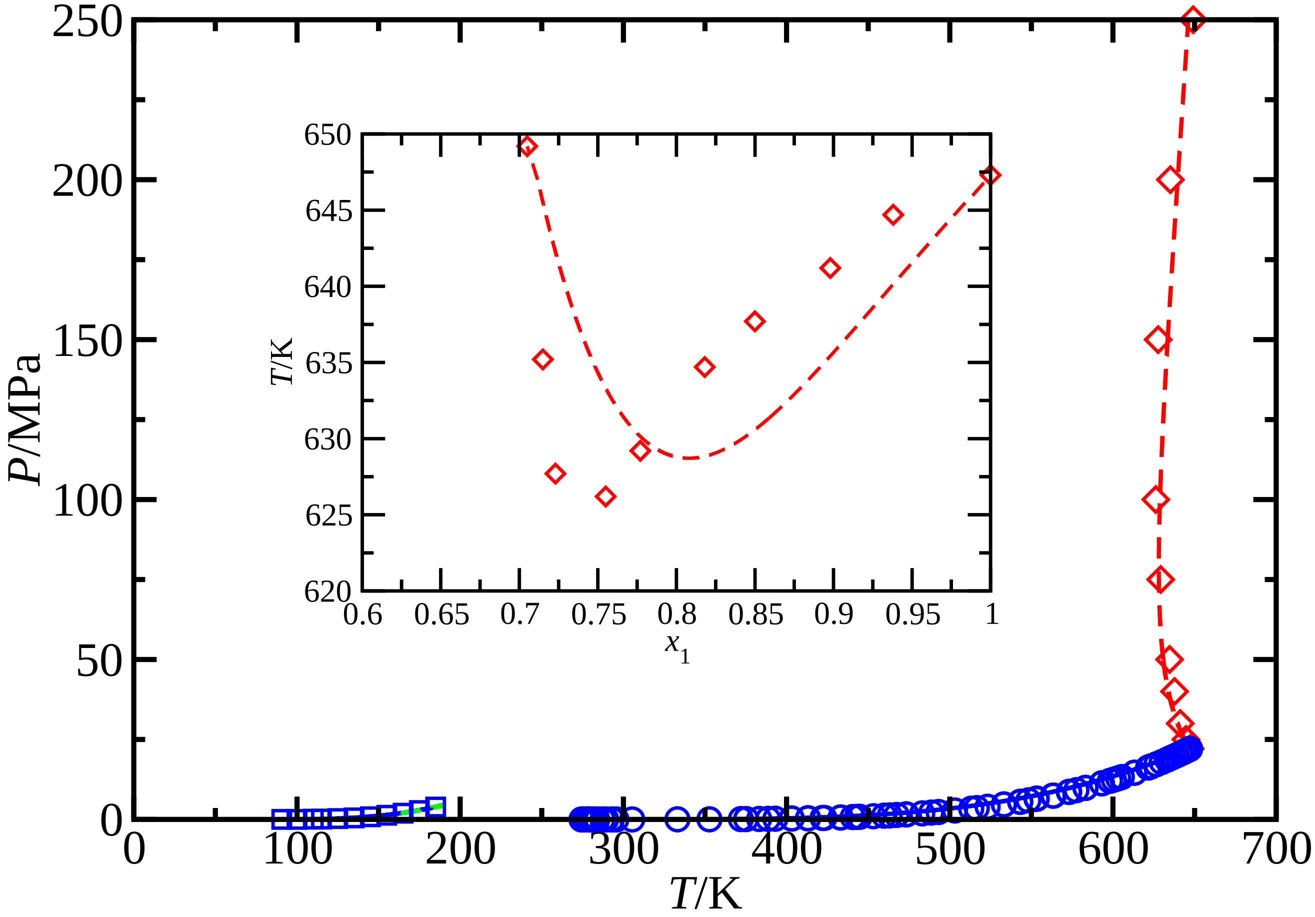

Figure 2: *PT* projection of the phase diagrama for the water(1) + methane(2) binary mixture. The circles to the experimental vapour pressure data of pure water,[50–58] the squares to the experimental vapour pressure of pure methane,[72] and the diamonds[68–71] to the experimental gas-liquid critical line at high temperature. The continuous curves are the SAFT-VR predictions for the vapour-pressures, the dashed curves for the critical lines and the long-dashed curve for the LLV three-phase line. The inset shows the *Px* projection of the gas-liquid critical line at high temperature of the mixture.

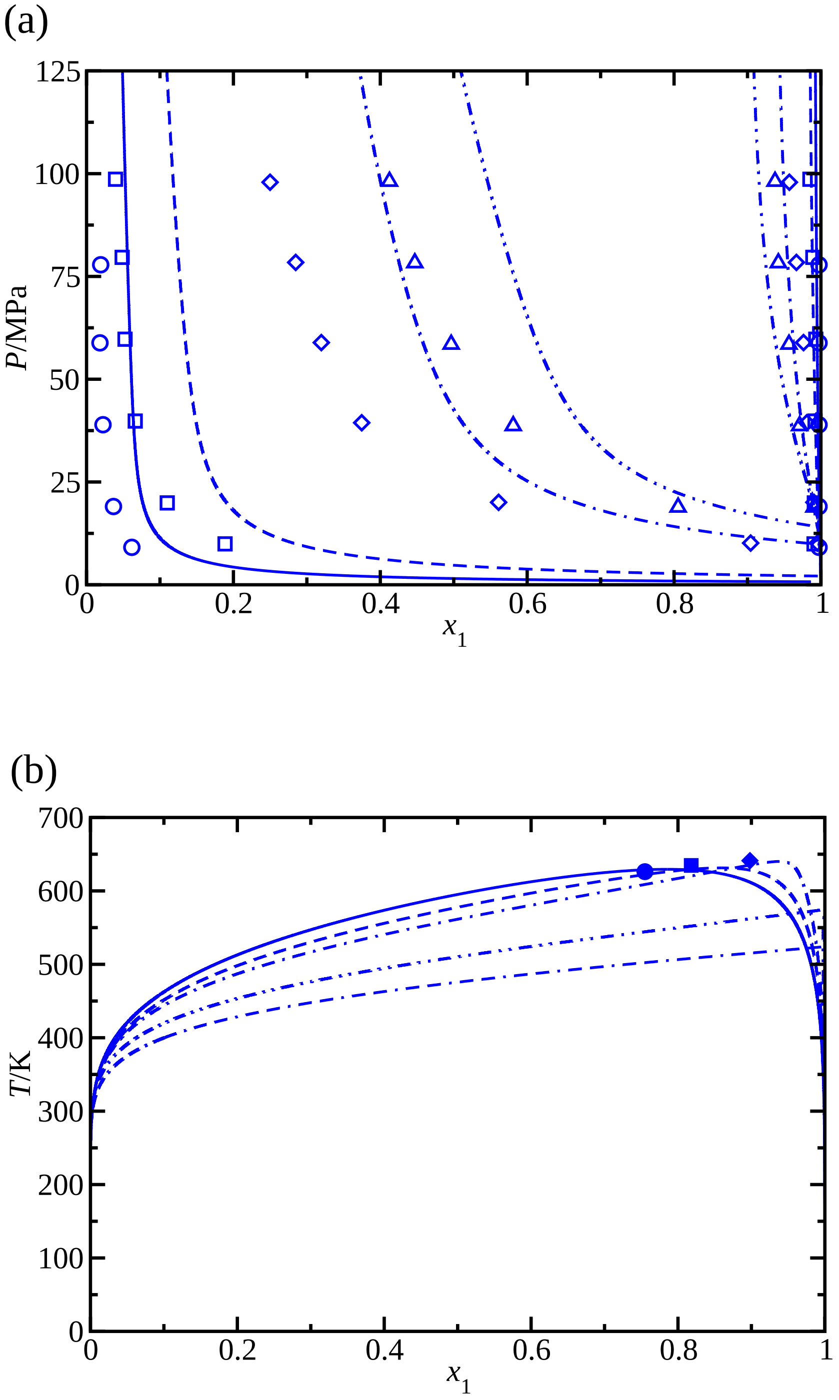

Figure 3: (a) *Px* and (b) *Tx* projection of the phase diagram for the water(1) + methane(2) binary mixture at different temperatures and pressures, respectively. The symbols correspond to the experimental data taken from the literature and the curves to the predictions obtained from SAFT-VR (a) at 423.15 K (circles[73] and continuous curves), 473.15 K (squares[73] and dashed curves), 573.15 K (diamonds[73] and dot-dashed curves), and 603.15 K (triangles[73] and dash-dash-dotted curves) and (b) at 100 MPa (circle[68–71] and continuous curve), 50 K (square[68–71] and dashed curve), 30 MPa (diamond[68–71] and dot-dashed curve), 10 K (dot-dot-dashed curve), and 5 MPa (dash-dash-dotted curve).

CH_4 + CO_2 binary mixture

The $CH_4 + CO_2$ binary mixture exhibits type I behaviour, with a continuous liquid vapour critical line connecting both pure compounds critical points, as shown in Figure 4. This critical locus presents a maximum, indicating large positive deviations from Raoult's law, a characteristic feature of binary mixtures presenting weak intermolecular interactions.

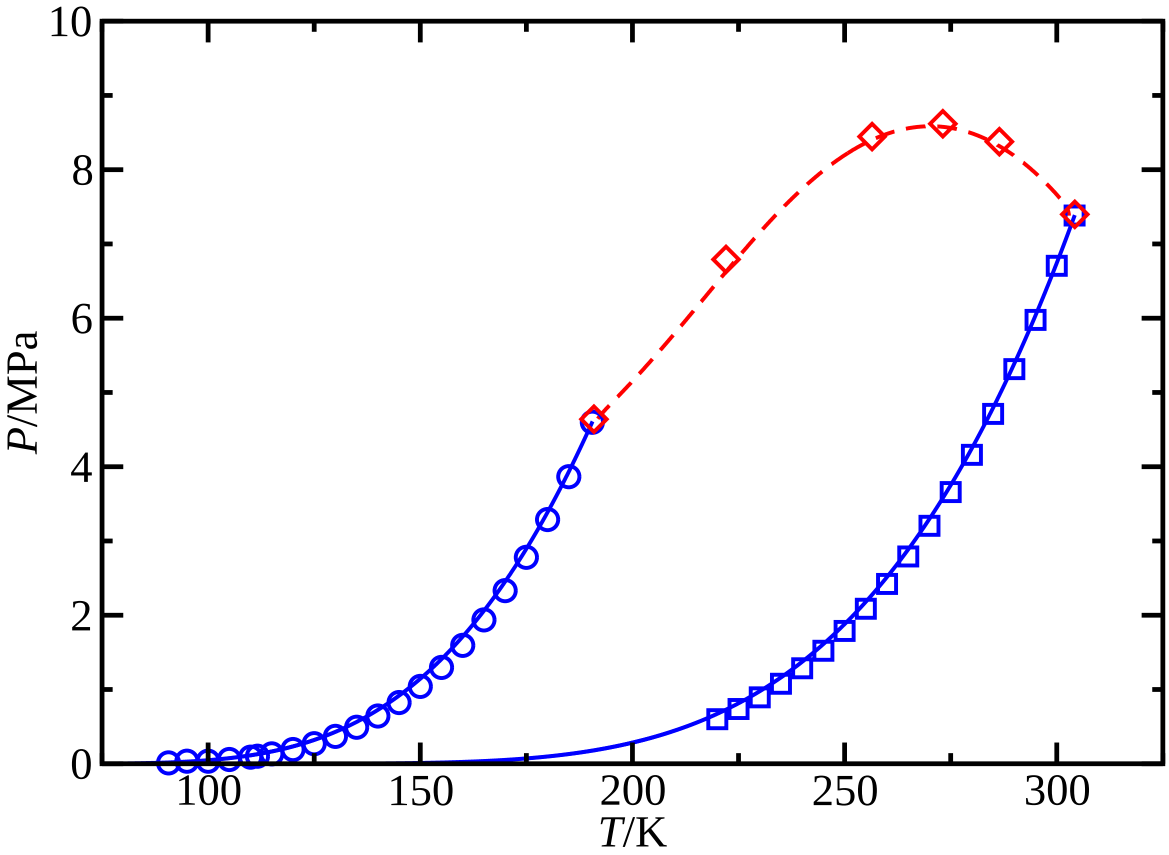

Figure 4: *PT* projection of the phase diagram for the methane(1) + carbon dioxide(2) binary mixture. The circles correspond to the experimental vapour pressure data of pure methane,[72] the squares to the experimental vapour pressure of pure carbon dioxide,[59–64] and the diamonds[22] to the experimental gas-liquid critical line. The continuous curves are the SAFT-VR predictions for the vapour-pressures and the dashed curves for the gas-liquid critical line.

Figure 5a shows the Px projection of the phase diagram, at temperatures ranging form 170 to 300 K, compared with the experimental data,[74,75] and the experimental critical line. Finally, the

Tx projection has been plotted in Figure 5b, together with the experimental data of Donnelly and Katz.[22] In both cases the theory reproduces accurately the vapour liquid equilibria of the binary, without considering any crossed interaction characteristic parameter.

$H_2O + CO_2 + CH_4$ ternary mixture

Once we have analyzed the phase behaviour of the three binary mixtures forming the $H_2O + CO_2 + CH_4$ ternary system, we have applied the SAFT-VR approach to obtain the phase behaviour of the ternary mixture at different thermodynamic conditions.

We first consider the phase behaviour of the mixture at similar conditions at which the system is found in tight-gas reservoirs. Figure 6a and Figure 6b show the triangular phase diagram of the mixture at 375.5 and 324.5 K, and different pressures, respectively. At these thermodynamic conditions, the CH_4 + CO_2 binary mixture exhibits a single fluid homogeneous phase (the critical point of CH_4 is located at 190.6 K and 4.61 MPa, and that corresponding to CO_2 at 304 K and 7.3 MPa). On the other hand, at 375.5 and 324.5 K and the pressures considered in Figure 6a and Figure 6b , the other two binary mixtures of the ternary system, i.e., H_2O + CO_2 and CH_4 + H_2O, exhibit the characteristic LL immiscibility of type III phase behaviour.

The theoretical predictions obtained from the SAFT-VR approach are compared with experimental data taken from the literature at different thermodynamic conditions. As it is shown, the theory is able to provide an excellent description of the phase behaviour. It is important to recall here that the results presented in Figure 6a and Figure 6b are pure predictions, since no further fitting has been performed. As it has been already explained, we have fitted the unlike binary interaction parameters associated to the $H_2O + CO_2$ dispersive interactions to experimental data taken from literature. Apart from that, no further experimental information from the ternary system has been used in the calculations presented in this work.

From the point of the phase envelopes of the binary mixtures involved it is easy to understant the phase diagrams shown in Figure 6a and Figure 6b, where the system exhibits large two-phase LL immiscibility regions. As previously mentioned, the $CH_4 + CO_2$ binary mixture is completely

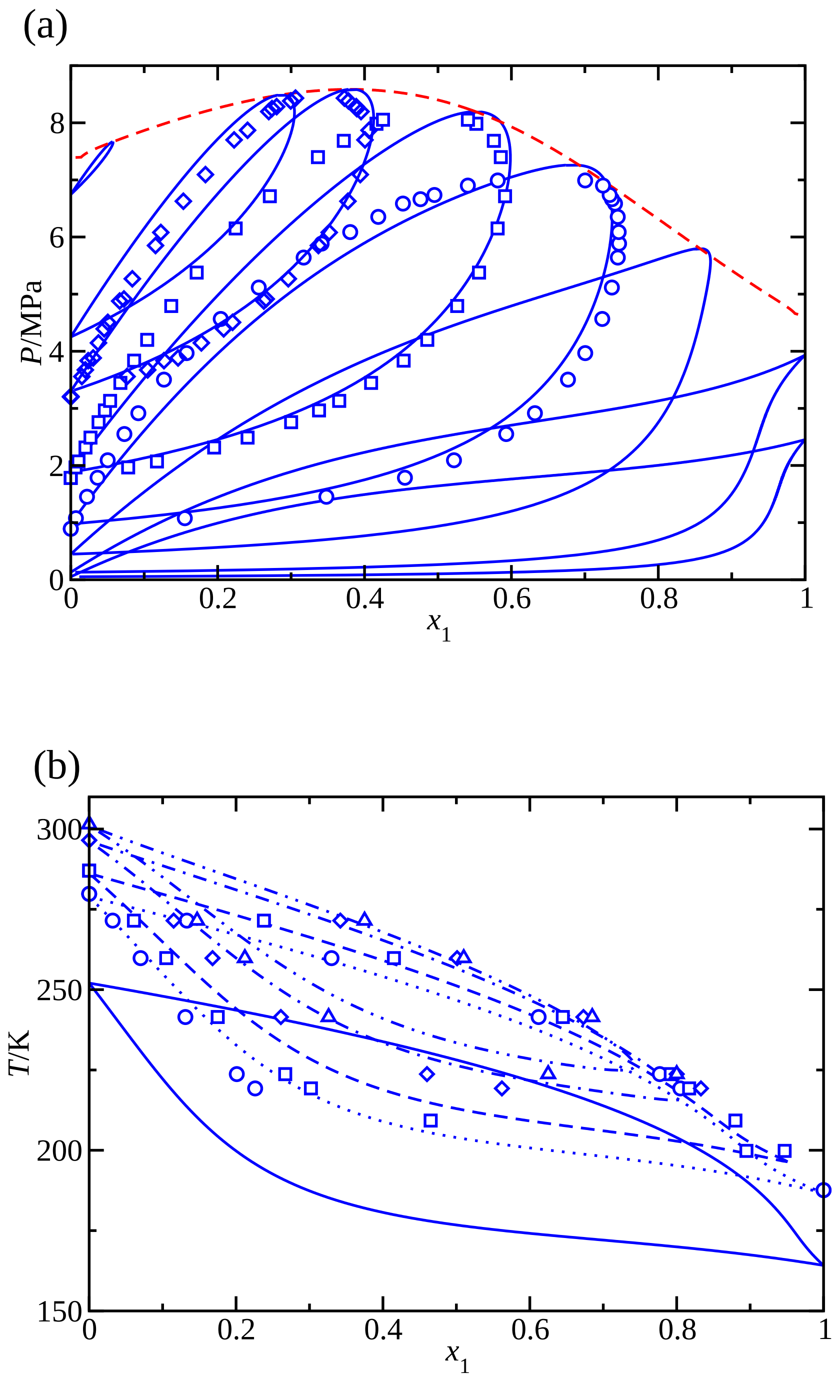

Figure 5: (a) *Px* and (b) *Tx* projections of the phase diagram for the methane(1) + carbon dioxide(2) binary mixture at different temperatures and pressures, respectively. The symbols correspond to the experimental data taken from the literature and the continuous curves to the predictions obtained from SAFT-VR: (a) at (from bottom to top) 170, 185, 210, 230 (circles[74]), 250 (squares[74]), 270 (diamonds[74,75]), and 300 K; (b) at 2 MPa (continuous curve), 4.137 MPa (circles[22] and dotted curve), 4.930 MPa (squares[22] and dashed curve), 6.206 MPa (diamonds[22] and dot-dashed curve), and 6.895 MPa (triangles[22] and dot-dot-dashed curve).

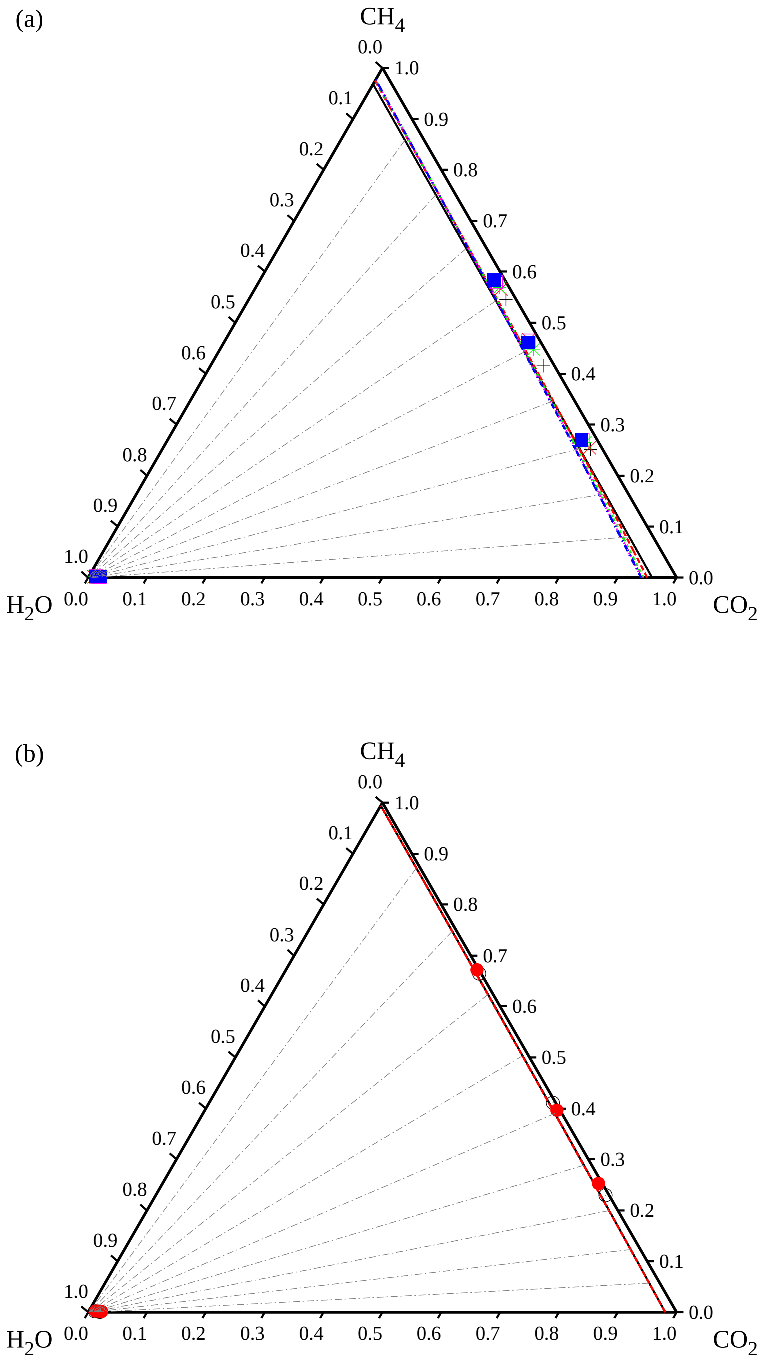

Figure 6: Ternary phase diagram of the mixture $H_2O(1) + CO_2(2) + CH_4(3)$ at different temperatures and pressures. The symbols correspond to the experimental data taken from the literature[25] and the curves to the predictions obtained from SAFT-VR at (a) 375.5 K and 10.5 MPa (pluses and continuous curves), 20.5 MPa (crosses and dashed curves), 30.3 MPa (stars and dotted curves), 40.2 MPa (open squares and dot-dashed curves), 50.0 MPa (filled square and dot-long dashed-dashed curves) and (b) 324.5 K and 30.5 MPa (open circles and continuous curves) and 50.0 MPa (filled circles and dashed curves).

miscible at these thermodynamic conditions, and this explains why the coexistence envelopes do not cut the CH_4-CO_2 axis of Figure 6a and Figure 6b. At $x_{CH_4} \approx 0$, which corresponds to a nearly pure H_2O + CO_2 binary system, the mixture exhibits LL immiscibility between a water-rich liquid phase ($x_{H_2O} \approx 0.98$) and a carbon dioxide-rich liquid phase ($x_{CO_2} \approx 0.95$). As the composition of the methane is increased, the relative composition of CO_2 in the CO_2-rich liquid phase decreases (the composition of the water-rich liquid phase is nearly constant and only varies from $x_{H_2O} \approx 0.98$ in the H_2O + CO_2 binary system to $x_{H_2O} \approx 0.99$ in the CH_4 + H_2O binary mixture, approximately) and changes continuously to a methane-rich liquid phase (with $x_{CH_4} \approx 0.95$ when $x_{CO_2} \approx 0$).

In order to explore in more detail the complex topology of the phase diagram of this ternary mixture, we have performed some additional calculations at different thermodynamic conditions, close to those at which the tight-gas reservoirs exist. We consider the effect of pressure on the phase behaviour of the system at the high-temperature region in Figure 7a. Since the vapour pressure of pure water at 500 K is 3.4 MPa, the ternary mixture exhibits LL immiscibility at all the pressures considered here. It is important to remember that aqueous mixtures of carbon dioxide and methane exhibit type III phase behaviour, and consequently, the corresponding ternary diagram should present at least one region of two-phase LL separation.

Figure 7a, shows the composition of one the liquid phases, i.e., the water-rich liquid phase, which is nearly constant as the pressure is reduced from 100 up to 5 MPa ($x_{H_2O} \approx 0.92$ at all the pressures). The composition of the other phase varies significantly as the pressure is decreased, from $x_{H_2O} \approx 0.2-0.3$ at the highest pressures ($20-100$ MPa), up to $x_{H_2O} \approx 0.4-0.5$ and $x_{H_2O} \approx 0.7-0.8$ at 10 and 5 MPa, respectively. It is obvious from the ensuing discussion that the size of the LL immiscibility region should decrease as the pressure is lowered, an expected behaviour in systems including one associative compound (H_2O).

We have also considered the effect of the temperature, at constant pressure, on the phase behaviour of the ternary mixture. As can be seen in Figure 7b, as the temperature is reduced from 500 up to 300 K approximately, the phase envelope corresponding to the water-poor liquid phase is shifted towards regions of lower compositions of H_2O, from $x_{H_2O} \approx 0.45$ up to $x_{H_2O} \approx 0.99$. This

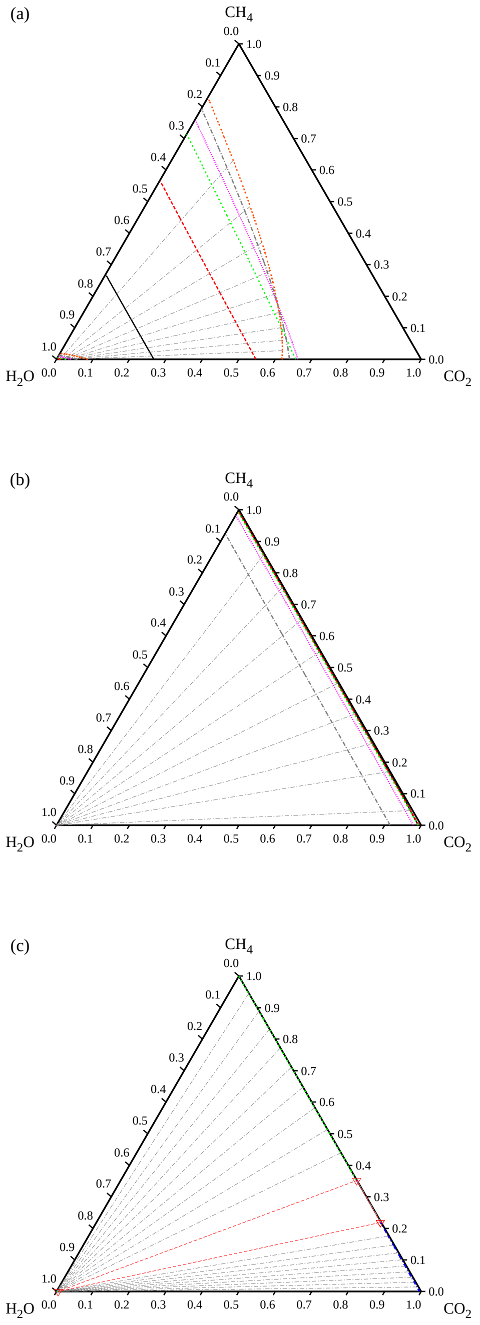

Figure 7: Ternary phase diagram of the mixture $H_2O(1) + CO_2(2) + CH_4(3)$ at different temperatures and pressures predictions obtained from SAFT-VR. (a) Two-phase liquid-liquid coexistence at 500 K and 5 MPa (continuous curves), 10 MPa (dashed curves), 20 MPa (dotted curves), 30 MPa (small-dotted curves), 50 MPa (dot-dashed curves), 100 MPa (tree-dot curves), and (b) two-phase liquid-liquid coexistence at 7.5 MPa and 300 K (continuous curves), 310 K (continuous curves), 320 K (continuous curves), 350 K (continuous curves), and 400 K (continuous curves), and (c) three-phase liquid-liquid-vapour coexistence at 7.5 MPa and 275 K. The dot-dashed lines in all parts of the figure correspond to the two-phase tie-lines at 100 MPa in (a), at 300 K in (b), and 275 K and 7.5 MPa in (c). The triangles correspond to the compositions of the three-phase liquid-liquid-vapour in coexistence in (c).

is a result of the increasing of the LL inmiscibility as the temperature decreases, as expected. On the contrary, the phase envelope corresponding to the water-rich liquid phase remains essentially at the same position in the triangular phase diagram as the temperature is decreased. This effect can be understood clearly from a molecular perspective: as the temperature decreases the association due to hydrogen bonding between water molecules increases, and as a consequence of this, the mutual solubility of water with carbon dioxide and methane decreases, resulting in larger LL immiscibility regions.

As we have seen in the previous figures, the phase behaviour of the system is dominated by relatively large LL immiscibility regions. The topology of the phase diagram at these thermodynamic conditions is characterized by a two-phase LL coexistence region, with one water-rich liquid phase and one water-poor liquid phase (which can be CO_2-rich or CH_4-rich liquid phase depending on composition). The phase envelope associated to the H_2O-rich liquid phase (close to the pure water corner of the triangular diagram) connects the CH_4-H_2O and H_2O-CO_2, whereas the other phase envelope, associated to the water-poor liquid phase (carbon dioxide- or methane-rich phase) connects the same axis in the opposite side of the phase diagram. In addition to the two-phase coexistence region, the phase diagram at high temperatures also exhibits a one-phase homogeneous region. As the temperature of the system decreases and/or the pressure is increased, the phase envelope associated to the H_2O-poor liquid phase approaches to the CH_4-CO_2 axis, as it has been shown previously in Figure 7a and Figure 7b. As a consequence, the two-phase LL immiscibility region increases, as expected, and the one-phase homogeneous region becomes smaller.

As we have discussed previously, the topology of this phase diagram (at these conditions) is a consequence of the $H_2O - CO_2$ and $H_2O - CH_4$ immiscibility. However, the ultimate reason why a one-phase homogeneous phase exists in the phase diagram is due to the miscibility at all proportions of CH_4 and CO_2, i.e., the CH_4 + CO_2 mixture does not exhibit LL neither VL phase separation. But, what does it happen if the temperature of the system is decreased, at the appropriate pressure, so that we ensure that the thermodynamic state of the mixture is located inside the VL coexistence region of the CH_4 + CO_2 binary mixture?

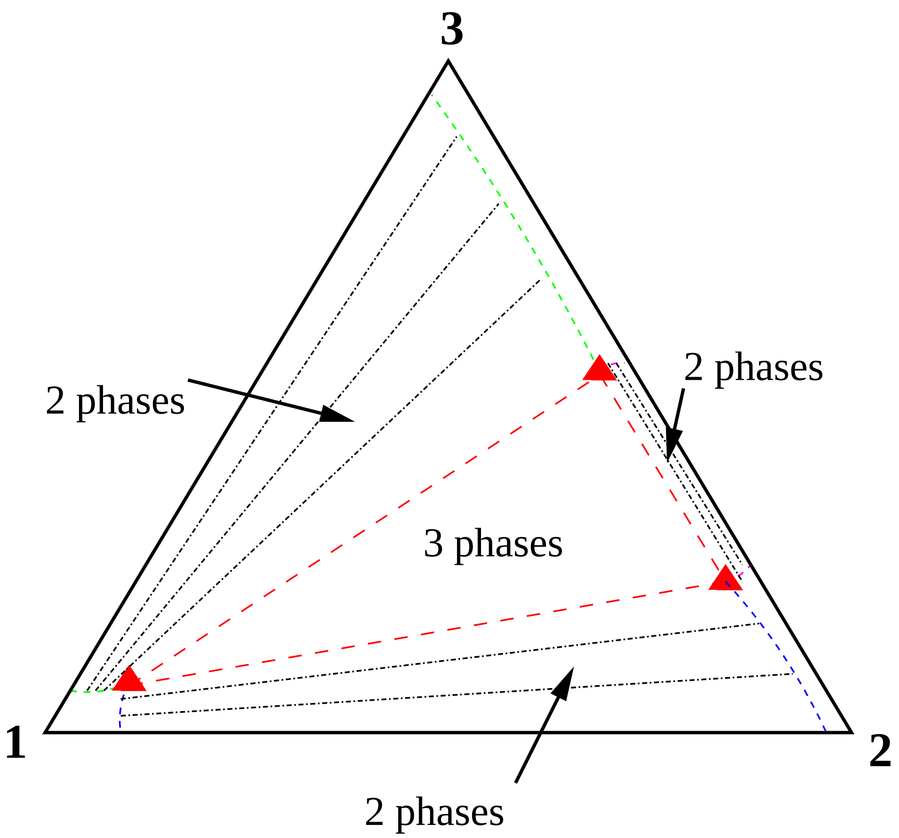

Figure 8: Schematic diagram of a hypothetical ternary mixture that exhibits three-phase separation (triangular region) and three two-phase regions associated to the binary mixtures 1–2, 2–3, and 1–3 of the ternary system. The red triangules represent the compositions of the three phases in coexistence, the red dashed lines the boundaries of this region, and the blue, green, and violet dashed lines the coexistence envelopes of the two-phase regions of the diagram. The dot-dashed lines inside of the three two-phase regions are the corresponding tie-lines. The zones located between the axis of the triangular diagram, the two-phase coexistence envelopes, and the three red triangles represent the one-phase regions of the phase diagram.

Figure 7c shows the triangular diagram of the $H_2O + CO_2 + CH_4$ ternary mixture at 275 K and 7.5 MPa. As it can be seen, the topology of the phase diagram is completely different than that shown in Figure 7a and Figure 7c, since it displays one central LLV three-phase region, three LL two-phase coexistence regions (two LL zones and one VL region), and three monophasic homogenous phases. Figure 8 shows a schematic diagram with the same topology than that exhibited by the mixture in Figure 7c.

One of the two-phase regions can not be distinguished due to its proximity to the $CH_4{-}CO_2$ axis of the diagram. The three one-phase homogenous regions, located near the vertexes of the triangular diagram, can not be seen neither due to the same reason, their very small size.

In the triangular central region two liquid phases coexist in equilibrium with a vapour phase. The compositions of each phase are defined by the coordinates of the central triangle in the phase diagram: the H_2O-rich liquid phase is composed by nearly pure H_2O ($x_{H_2O} \approx 0.996$), with a liquid-like packing fraction $\eta_{L_1} \approx 0.49$, the second liquid phase is formed by a mixture of CO_2 ($x_{CO_2} \approx 0.778$) and CH_4 ($x_{CH_4} \approx 0.210$), with a liquid-like packing fraction $\eta_{L_2} \approx 0.22$, and the vapour phase, with a composition of $x_{CO_2} \approx 0.647$ and $x_{CH_4} \approx 0.351$), and a vapour-like packing fraction $\eta_V \approx 0.11$.

This behaviour can be explained from a molecular perspective: the $H_2O - CH_4$ and $H_2O - CO_2$ interactions are very unfavourable due to self-association between H_2O molecules (these mixtures exhibit LL immiscibility). At high temperatures and pressures, since the CH_4 + CO_2 mixture exhibits only a homogeneous liquid phase, the ternary system minimizes its free energy by segregating the system into a water-rich liquid phase, dominated by hydrogen bonding interactions, and a second water-poor liquid phase, dominated by the dispersive interactions. This second liquid phase changes its methane-rich to carbon dioxide-rich character according to the relative $H_2O - CO_2$ and $H_2O - CH_4$ affinity at the corresponding pressures and temperatures. However, at low temperatures and pressures, the CH_4 + CO_2 mixture exhibits VL phase separation. This region eventually interacts with the LL two-phase region dominated by hydrogen bonding, resulting in the new topology shown in Figure 7c.

Due to the proximity of the LLV three-phase region to the triangular axis of the diagram it is difficult to distinguish clearly the exact location of the coexistence regions. Figure 8 shows a schematic diagram with the same topology than that exhibited by the mixture presented in Figure 7c. As can be seen, the system has a central three-phase coexistence region. Each of the sides of the triangular region connects three two-phase regions with the corresponding two-component coexistence axis, indicating that the three binary mixtures that form the ternary system exhibit two-phase separation at these thermodynamic conditions. In the particular case of the mixture shown in Figure 7c, the H_2O + CO_2 and + CH_4 binary mixtures exhibit LL separation and the last mixture (CO_2 + CH_4) presents VL coexistence at the particular thermodynamic conditions.

As we have mentioned, the proximity of the three-phase region to the triangular axis of the phase diagram, which is a consequencie of the large LL immiscilibity regions exhibited by two of the three binary mixtures that form the system (H_2O + CO_2 and + CH_4 binary mixtures) and the low mutual solubilities between water and carbon dioxide and methane, makes really difficult to see if the system really exhibits three-phase separation. We have included two additional figures that help to understand the phase behaviour exhibited by the same at the same thermodynamic conditions presented in Figure 7c. Figure 9 shows the carbon dioxide composition and the water composition *versus* the methane composition at the same conditions as those presented in Figure 7c. As can be seen, the blue, red, and violet curves are the phase enveloped associated to the two-phase coexistence regions previously shown in the triangular diagram of Figure 7c, which end at the vertex of the triangular region (red triangles in this figure) and at the three axis of the triangular diagram.

We have also analized the phase behaviour of the ternary mixture at low temperatures, with particular emphasis on the effect of temperature and pressure on the three-phase LLV immiscibility region. Figure 10 shows the effect of pressure, at six different temperatures on the three-phase triangular region. The three two-phase regions and the three one-phase homogenous phases have not been displayed in these representations for the sake of clarity. However, all the phases involved at each temperature and pressure shown in this figure are topologically equivalent to that of Fig-

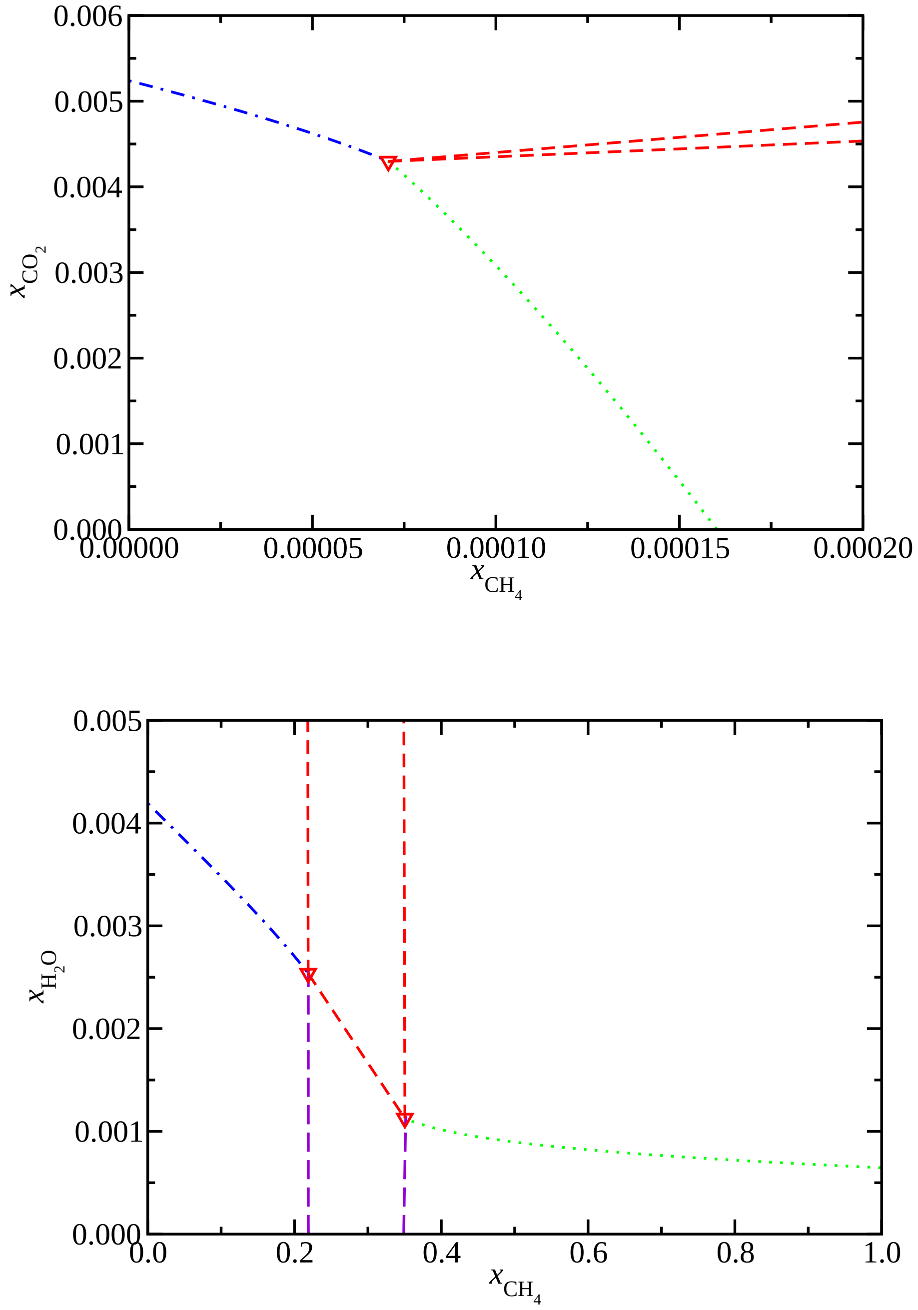

Figure 9: (a) Carbon dioxide and (b) water compositions as functions of the methane composition of the ternary mixture $H_2O(1) + CO_2(2) + CH_4(3)$ at 7.5 MPa and 275 K. The blue dot-dashed curves represent the LL phase envelope associated to the CH_4-poor two-phase region, the green dot-dashed curves the LL phase envelope associated to the CO_2-poor two-phase region, and the violet dotted curves the VL phase envelope associated to the H_2O-poor two-phase region. These three two-phase regions are associated to the regions connecting the CO_2–CH_4, H_2O–CH_4, and the CO_2–CH_4 axis in Fig. 7c. The red triangles are the compositions of the three-phase LLV in coexistence and the red dashed lines are the boundaries of the three-phase region in the diagram. We have used here the same colours and symbols than in Fig. 7c.

ure 8. As it can be seen in Figure 10a, at 275 K, the LLV three-phase region decreases in size as the pressure is increased, as expected from the previous discussion. In particular, the two phases near the CH_4-CO_2 axis of the phase diagram, i.e., the water-poor liquid phase and the CO_2-rich vapour phase, become more similar as the pressure is increased. At 8.60 MPa approximately, both phases become critical in the presence of the second (water-rich) liquid phase. At pressures above 8.60 MPa approximately, the system exhibits LL two-phase separation, as we have seen previously in Figure 7b.

When the temperature is raised, the same qualitative behaviour is observed. However, the LLV three-phase region becomes smaller as temperature increases, as expected. At the lowest pressure (7.5 MPa), the triangular region of coexistence becomes narrower as the temperature is near 300 K. In addition, the range in pressures at which the LLV three-phase region is stable decreases as temperature increases. For instance, at 295 K, the pressure at which the three-phase coexistence vanishes is below 8 MPa, whereas at 300 K, the pressure value is equal to 7.66 MPa, which means that the range at which the three phases coexist is smaller than 0.2 MPa.

All the plots shown in Figure 10 have a common feature: when the pressure is increased, the system exhibiting three phases in coexistence evolves to show two-phase equilibrium phase behaviour, or in other words, the system crosses a critical endpoint. In binary mixtures (of fluids), a critical endpoint is the endpoint of a three-phase line in which two of the phases become critical in the presence of the third phase in coexistence. For instance, mixtures exhibiting LL immiscibility (types II, III, IV, V, and VI) have at least one critical endpoint (mixtures of type VI have two critical endpoints and mixtures of type IV have three). There exist two different natures of critical endpoints depending on the two phases that become critical: (1) critical endpoint of nature $L_1 = L_2 + V$, in which the two liquid phases are critical in the presence of a vapour phase; and (2) critical endpoint of nature $L_1 = V + L_2$, i.e., the liquid phase 1 and the vapour phase V are critical in the presence of the liquid phase 2. In particular, the second type of critical endpoint appears as an upper critical endpoint in mixtures that exhibit type III phase behaviour, as in the H_2O + CO_2 and $H_2O + CH_4$ binary mixtures studied in this work.

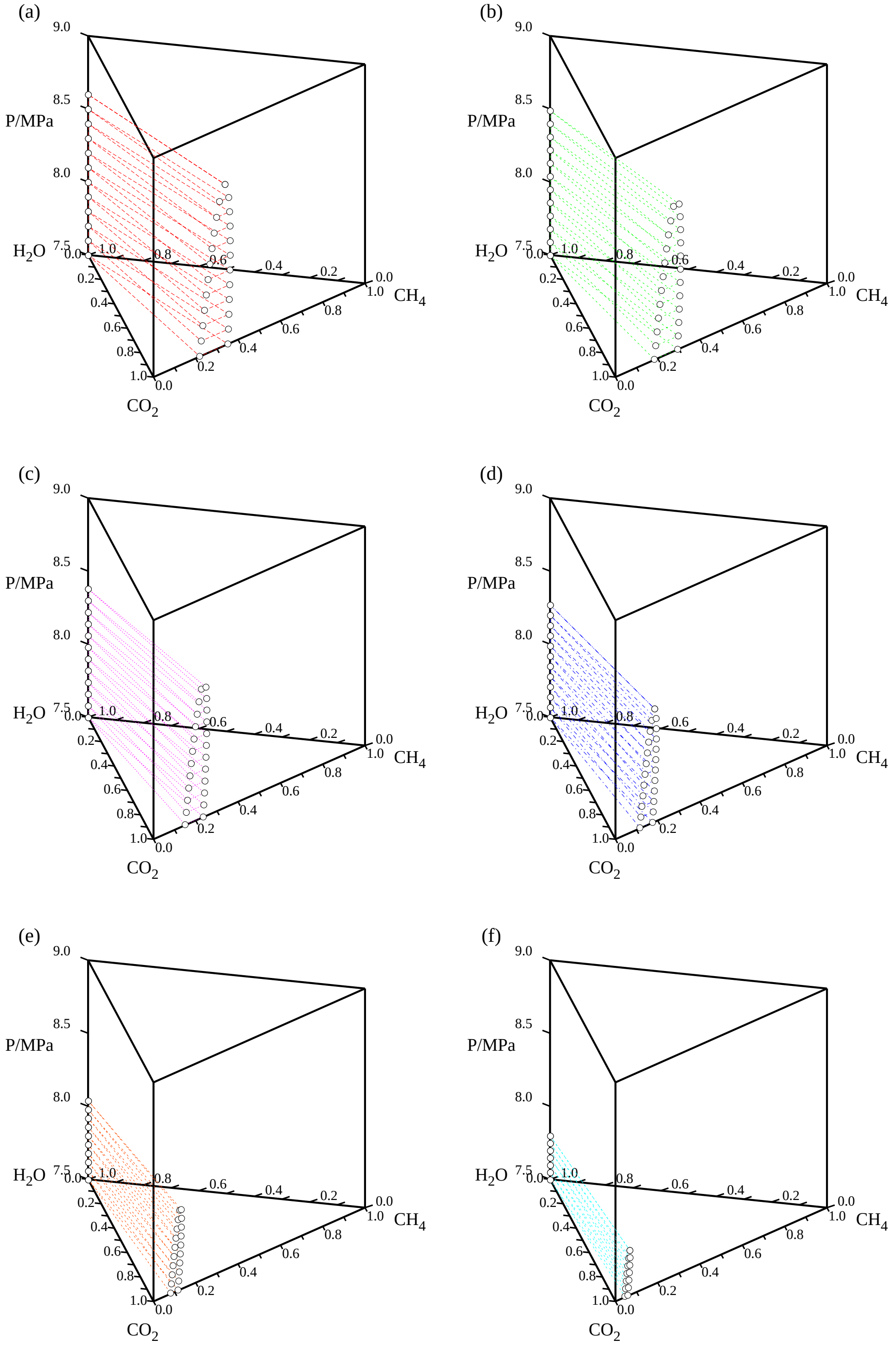

Figure 10: Tridimensional view of the ternary diagram, as a function of pressure, of the mixture $H_2O(1) + CO_2(2) + CH_4(3)$ as predicted from SAFT-VR at 275 K (a), 275 K (b), 280 K (c), 290 K (d), 295 K (e), 300 K (f). The dashed lines represent the sides of the triangles that bound the three-phase LLV coexistence region and the circles their corresponding compositions. The existing two-phase liquid-liquid and two-phase vapour-liquid coexistence curves, as well as the their corresponding tie-lines are not included to clarify the graphs.

According to the rule phase, critical endpoints are states with zero degress of freedom, which means that they are fixed points in the corresponding phase diagram. However, in ternary mixtures, due to the presence of an additional component, the three-phase states lie on a surface (in the multidimensional thermodynamic phase space), instead of a line (as it occurs in binary mixtures), and consequently, the critical endpoint states are not longer fixed points in the phase diagram, but lie along a line, i.e., along critical endlines.

We have determined from SAFT-VR the upper critical endpoint temperatures and pressures, as function of the CO_2 mole fraction on a H_2O free basis, i.e., $x^*_{CO_2} = x_{CO_2}/(x_{CO_2} + x_{CH_4})$. As can be seen in Figure 11 , a continuous critical endpoing locus (in the Px^* and Tx^* projections of the phase diagram) of nature $L_2 = V + L_1$ separates the three-phase surface L_1L_2V (lower temperature part of the diagrams) from a two-phase region L_1L_2 (higher temperature part of the diagram). It should be noted that the limit $x^*_{CO_2} = 0$ represents the upper critical endpoint of the binary mixture H_2O(1) + CH_4(2) and the limit $x^*_{CO_2} = 1$ the upper critical endpoint of the binary mixture H_2O(1) + CO_2(2). In fact, this figure can be understood better in the context of pseudobinary mixtures, i.e., the H_2O(1) + CH_4(2)+ CO_2(3) ternary mixture can be viewed as a binary mixture of H_2O and a second pseudocomponent, which is a mixture of CO_2 and CH_4 controlled by the mole fraction $x^*_{CO_2}$. Under this point of view, the upper critical endpoint of the H_2O(1) + CH_4(2) real binary mixture, at $x^*_{CO_2} = 0$, 190.6 K, and 4.6 MPa, changes continuously to the second H_2O(1) + CO_2(2) real binary mixture, at $x^*_{CO_2} = 1$, 305.4 K, and 7.46 MPa, as the mole fraction $x^*_{CO_2}$ is increased.

Finally, we have also considered the effect of temperature, at six different temperatures on the three-phase triangular region. As can be seen in Figure 10 , the three-phase coexistence region decreases in size as the temperature rises. As the pressure varies from 6 up to 7.5 MPa, the same qualitative behaviour is observed, although the temperature at which the system passes from a three-phase to a two-phase behaviour increases. This trend is clearly reversed for the two highest pressures, 8 and 8.5 MPa. It should be noted that at pressure $6 - 7.5$ MPa the system does not exhibits critical behaviour, i.e., the system passes from a three-phase to a two-phase region without crossing a critical endpoint, as can be seen clearly in Figure 9b (close to the $x^*_{CO_2} \approx 0$ region). In

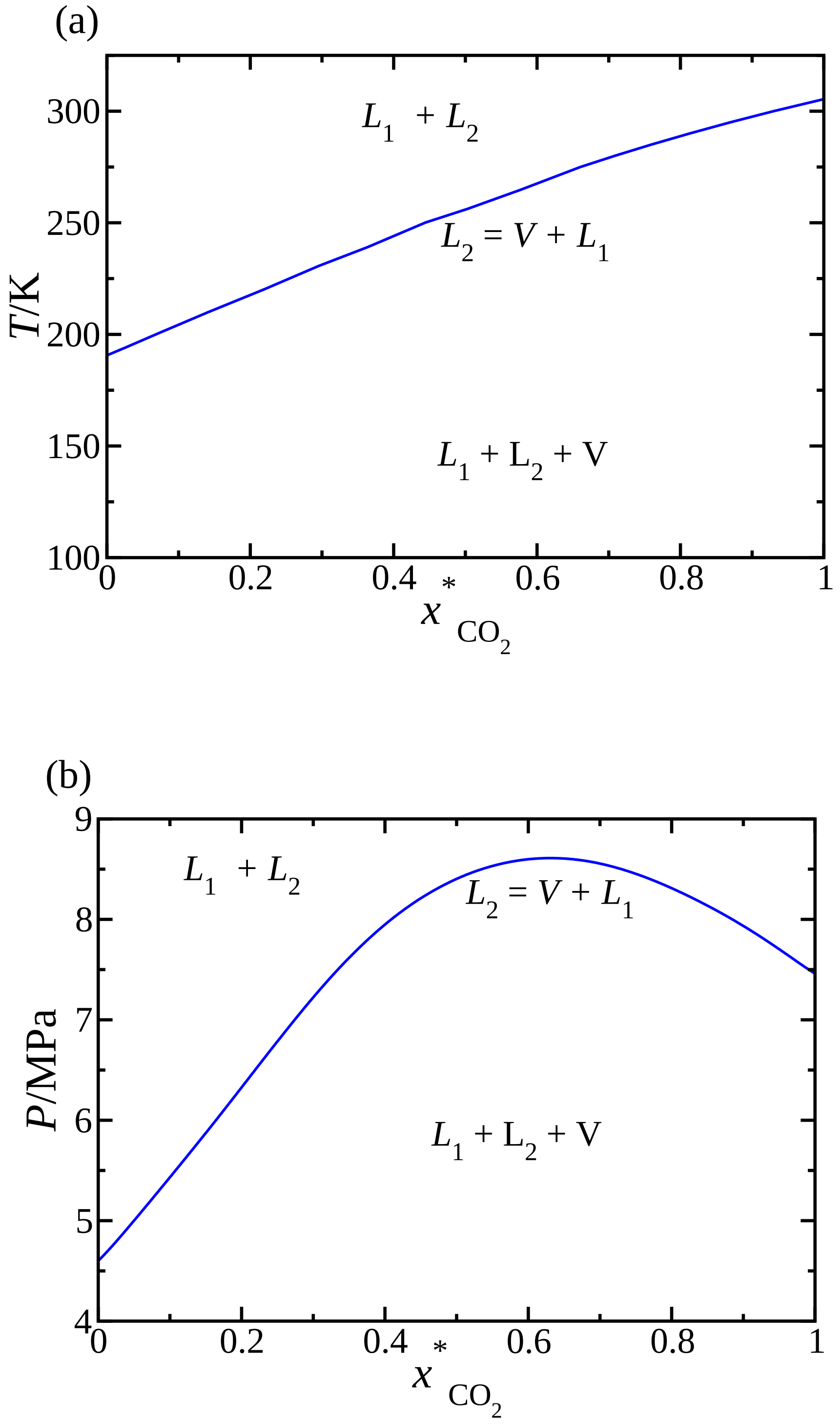

Figure 11: Upper critical endpoint temperatures (a) and pressures (a) as functions of the mole fraction of $x^*_{CO_2}$, the carbon dioxide mole fraction free basis.

other words, the critical endpoint pressures of the ternary mixture close to the $x^*_{CO_2} \approx 0$ region, or equivalently, close to the region of the upper critical endpoint of the $H_2O(1)$ + CO_2 real binary mixture, are always higher than 7.5 MPa. As a consequence of this, at pressures below 7.5 MPa, the system passes from the L_1L_2V three-phase region to the L_1L_2 surface without crossing a critical endpoint. This change of behaviour is due to the presence of the vapour pressure curve of pure CO_2 in this region: when the temperature of the system is decreased at the pressure is below ~ 7.5 MPa (the critical pressure of CO_2 is 7.3 MPa approximately), the system crossed the vapour pressure curve of pure CO_2 and the ternary systems passes directly (not critically) from the three-phase to the two-phase region. Although this mechanism might seem peculiar, a similar scenario occurs in binary mixtures when the system crosses the vapour pressure curve of one of the components from the two-phase to the one-phase region.

Conclusions

The results described in the precedent section, that include a detailed description of the global phase behaviour of this ternary mixture are a proof of the ability of the SAFT$-$VR EoS to describe remarkably complex phase equilibria using only a reduced number of molecular based characteristic parameters. It has been shown that, for the set of binary mixtures involved, only the H_2O $+CO_2$ one demanded the determination of an unlike interaction energy combining rule parameter, with the aim to improve the estimation of the minimum of the high temperature branch of the discontinuous LV critical line, a feature that is characteristic of its type III binary phase diagram. Nevertheless, the purely predictive results obtained for the other aqueous binary did not need any supplementary mixing parameter determination, and the calculations obtained from the pure component parameters yielded fairly good results if compared with experimental data. The same situation holds for the simpler type I CH_4 $+CO_2$ binary mixture.

Once these preliminary results on the constituent binary mixtures were obtained, it must be recalled that the rest of the phase equilibria calculations presented here were performed without

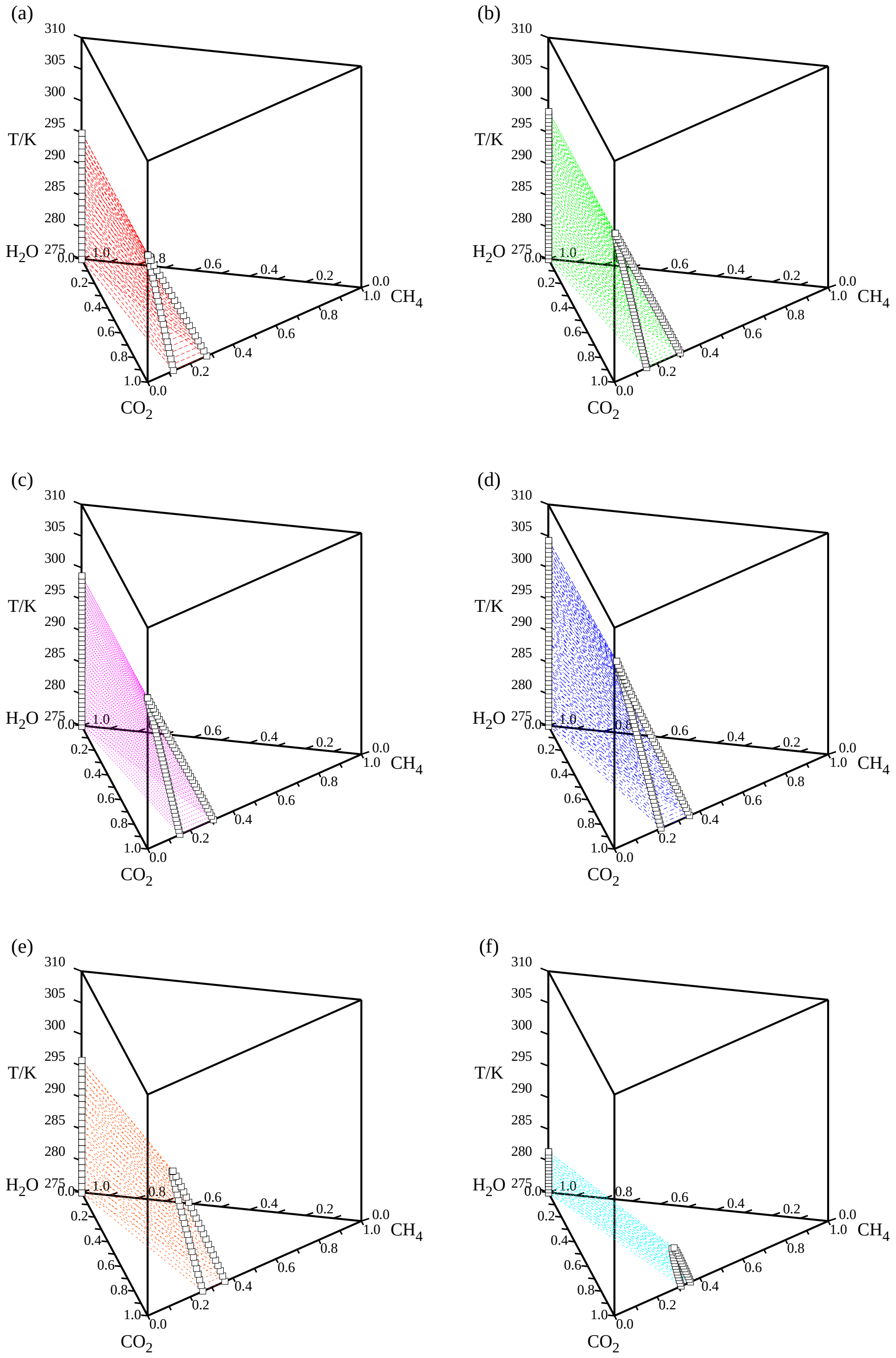

Figure 12: Tridimensional view of the ternary diagram, as a function of temperature, of the mixture $H_2O(1) + CO_2(2) + CH_4(3)$ as predicted from SAFT-VR at 6 MPa (a), 6.5 MPa (b), 7 MPa (c), 7.5 MPa (d), 8 MPa (e), 8.5 MPa (f). The dashed lines represent the sides of the triangules that bound the three-phase LLV coexistence region and the squares their corresponding compositions. The existing two-phase liquid-liquid and two-phase vapour-liquid coexistence curves, as well as the their corresponding tie-lines are not included to clarify the graphs.

fitting any supplementary parameter. This fact underlines the predictive power of SAFT-VR EoS when applied to the estimation of complex multicomponent phase equilibria landscapes, a matter of primary importance for applied purposes that has not received enough attention in the literature although it constitutes a demanding challenge for any thermodynamic model.

Our attention has then been focused on the pressure and temperature ranges of interest in the application that motivated this work, i. e., the thermodynamic conditions that are presumed to occur in tight gas reservoirs. The obtained phase equilibria behaviour for the ternary mixture is a result of the competition of the wide high pressure liquid liquid separation regions, typical of the binary aqueous mixtures, and the effect induced at lower pressures by the $CH_4 + CO_2$ liquid vapour critical curve. This combination of two type III and one type I binary mixtures led to the appearance of two clearly differenced regions. At pressures above the maximum of the $CH_4 + CO_2$ LV critical line, the ternary diagrams obtained show a wide region of LL equilibria, and an homogeneous phase close to the completely miscible (in these conditions) $CH_4 + CO_2$ mixture. This is a direct consequence of the well known high pressure LL equilibria obtained previously for both aqueous binaries. The boundaries of this LL separation region agrees well with the available experimental data, and the effect of temperature and pressure has been shown and rationalized according to the mutual interactions between the three molecules present.

This first scenario of phase behaviour for the ternary mixture changes abruptly in the temperature and pressure range where the $CH_4 + CO_2$ shows LV equilibria. In this range of conditions, the wide LL gap in the ternary diagram is transformed into a situation where a central three phase LLV equilibria region, three LL equilibria regions, and three tiny monophasic regions placed closer to each pure compound coexist. So, for these temperature and pressure combinations, a modification in the mixture composition can lead to one, two or three phases in equilibrium. The topology of this LLV three phase equilibrium region has been then explored, by performing calculations at different temperature and pressure values. The aim now was to locate in every case the three phase to two phase equilibrium transition coordinates, this is, the critical endpoints for the ternary mixture, that, contrarily to what happens in binary mixtures, lie along a line connecting the upper critical endpoints of both aqueous binary mixtures. Thus, this ternary critical endpoint line, of nature $L_1 = V + L_2$, has been traced and its trend plotted against temperature and pressure. Nevertheless, this transition from ternary three phase to two phase equilibria in the mixture may occur as well directly (without crossing a critical endpoint), and the transition is produced crossing the saturation curve of one of the pure compounds, CO_2 in this case.

This final summary depicts a complex and rather unexpected phase behaviour for this ternary mixture, which emphasizes the need to handle versatile and robust theoretical models when any related practical application is envisaged. SAFT-VR has shown here again its suitability to reproduce the existing phase equilibria experimental data with remarkable accuracy, offering also estimations of the phase equilibria trend of the mixture over wide ranges of temperature and pressure. All this is obtained on a molecular basis, with transferable parameters that may be applied to estimate an additional large ensemble of thermodynamic or even interfacial properties if needed.

Acknowledgement

J. M. M. and M. M. P. acknowledge Consellería de Educación e Ordenación Universitaria (Xunta de Galicia) and Ministerio de Ciencia e Innovación (Proj. Ref. FIS2009-07923, and FPU grant Ref. AP2007-02172), in Spain, for financial support.

References

(1) Schmoker, J. W. *AAPG Bull.* **2002**, *86*, 1993–1999.

(2) Ahmed, T.; McKinney, P. *Advanced Reservoir Engineering*; Gulf. Prob. Pub., 2005; p p 233 ss.

(3) Dubessy, J.; Buschaert, S.; Lamb, W.; Pironon, J.; Thiéry, R. *Chem. Geol.* **2001**, *173*, 193–205.

(4) Goel, N. *J. Petrol. Sci. Eng.* **2006**, *51*, 169–184.

(5) Gil-Villegas, A.; Galindo, A.; Whitehead, P. J.; Mills, S. J.; Jackson, G.; Burgess, A. N. *J. Chem. Phys.* **1997**, *106*, 4168–4186.

(6) Galindo, A.; Davies, L. A.; Gil-Villegas, A.; Jackson, G. *Mol. Phys.* **1998**, *93*, 241–252.

(7) dos Ramos, M. C.; Blas, F. J.; Galindo, A. *Fluid Phase Equilibria* **2007**, *261*, 359–365.

(8) dos Ramos, M. C.; Blas, F. J.; Galindo, A. *J. Phys. Chem. C* **2007**, *111*, 15924–15934.

(9) Blas, F. J.; Galindo, A. *Fluid Phase Equilibria* **2002**, *194*, 501–509.

(10) Galindo, A.; Blas, F. J. *J. Phys. Chem. B* **2002**, *106*, 4503–4515.

(11) Clark, G. N. I.; Haslam, A.; Galindo, A.; Jackson, G. *Mol. Phys.* **2006**, *104*, 3561–3581.

(12) Scott, R. L.; van Konynenburg, P. H. *Discuss. Farad. Soc.* **1970**, *49*, 87–97.

(13) van Konynenburg, P. H.; Scott, R. L. *Philos. Trans. A* **1980**, *298*, 495–540.

(14) Spycher, N.; Pruess, K.; Ennis-King, J. *Geochim. Cosmochim. Acta* **2003**, *67,* 3015–3031.

(15) Valtz, A.; Chapoy, A.; Coquelet, C.; Paricaud, P.; Richon, D. *Fluid Phase Equilibria* **2004**, *226*, 333–344.

(16) Pappa, G.; Perakis, C.; Tsimpanogiannis, I. N.; Voutsas, E. *Fluid Phase Equilibria* **2009**, *284*, 56–63.

(17) Sun, R.; Dubessy, J. *Geochim. Cosmochim. Acta* **2010**, *74*, 1982–1998.

(18) Lafitte, T.; Mendiboure, B.; Piñeiro, M. M.; Bessières, D.; Miqueu, C. *J. Phys. Chem. B* **2010**, *114*, 11110–11116.

(19) Lafitte, T.; Piñeiro, M. M.; Daridon, J.-L.; Bessières, D. *J. Phys. Chem. B* **2007**, *111*, 3447–3461.

(20) Breil, M. P.; Tsivintzelis, I.; Kontogeorgis, G. M. *Fluid Phase Equilibria* **2011**, *301*, 1–12.

(21) Galindo, A.; Whitehead, P. J.; Jackson, G.; Burgess, A. N. *J. Phys. Chem.* **1996**, *100*, 6781–6792.

(22) Donnelly, H. G.; Katz, D. L. *Ind. Eng. Chem.* **1954**, *46*, 511–517.

(23) Dhima, A.; de Hemptinne, J.; Jose, J. *Ind. Eng. Chem. Res.* **1999**, *38*, 3144–3161.

(24) Jarne, C.; Blanco, S. T.; Gallardo, M. A.; Rauzy, E.; Otín, S.; Velasco, I. *Energy Fuels* **2004**, *18*, 396–404.

(25) Qin, J. F.; Rosenbauer, R. J.; Duan, Z. *J. Chem. Eng. Data* **2008**, *53*, 1246–1249.

(26) Seo, Y.-T.; Lee, H. *J. Chem. Eng. Data* **2001**, *46*, 381–384.

(27) Duan, Z.; Moller, N.; Weare, J. H. *Geochim. Cosmochim. Acta* **1992**, *56*, 2619–2631.

(28) Austegard, A.; Solbraa, E.; de Koeijer, G.; Molnvik, M. J. *Chem. Eng. Res. and Des.* **2006**, *84(A9)*, 781–794.

(29) Soave, G. *Chem. Eng. Sci.* **1972**, *27*, 1197–1203.

(30) Kontogeorgis, G. M.; Voutsas, E.; Yakoumis, I. V.; Tassios, D. P. *Ind. Eng. Chem. Res.* **1996**, *35*, 4310–4318.

(31) Bol, W. *Mol. Phys.* **1982**, *45*, 605–616.

(32) Nezbeda, I.; Kolafa, J.; Kalyuzhnyi, Y. *Mol. Phys.* **1989**, *68*, 143–160.

(33) Patel, B. H.; Paricaud, P.; Galindo, A.; Maitland, G. C. *Ind. Eng. Chem. Res.* **2003**, *42*, 3809–38234.

(34) Ji, X.; Tan, S. P.; Adhidarma, H.; Radosz, M. *Ind. Eng. Chem. Res.* **2005**, *44*, 8419–8427.

(35) Hansen, J. P.; McDonald, I. R. *Theory of simple liquids*; Academic Press: London, 1990.

(36) Barker, J. A.; Henderson, D. J. *J. Chem. Phys.* **1967**, *47*, 2856.

(37) Barker, J. A.; Henderson, D. J. *J. Chem. Phys.* **1967**, *47*, 4714.

(38) Barker, J. A.; Henderson, D. J. *Rev. Mod. Phys.* **1976**, *48*, 587–671.

(39) Boublik, T. *J. Chem. Phys.* **1970**, *53*, 471–472.

(40) Barker, J. A.; Henderson, D. J. *Rev. Mod. Phys.* **1971**, *54*, 1523.

(41) Chapman, W. G. *J. Chem. Phys.* **1990**, *93*, 4299–4304.

(42) Wertheim, M. S. *J. Stat. Phys.* **1984**, *35*, 19–34.

(43) Wertheim, M. S. *J. Stat. Phys.* **1984**, *35*, 35–47.

(44) Wertheim, M. S. *J. Stat. Phys.* **1986**, *42*, 459–476.

(45) Wertheim, M. S. *J. Stat. Phys.* **1986**, *42*, 477–492.

(46) Jackson, G.; Chapman, W. G.; Gubbins, K. E. *Mol. Phys.* **1988**, *65*, 1–31.

(47) Chapman, W. G.; Gubbins, K. E.; Jackson, G.; Radosz, M. *Ind. Eng. Chem. Res.* **1990**, *29*, 1709–1721.

(48) Chapman, W. G.; Jackson, G.; ; Gubbins, K. E. *Mol. Phys.* **1988**, *65*, 1057–1079.

(49) Forte, E.; Llovell, F.; Vega, L. F.; Trusler, J. P. M.; Galindo, A. *J. Chem. Phys.* **2011**, *134*, 154102.

(50) Apelblat, A. J. *J. Chem. Thermodyn.* **1999**, *31*, 869–893.

(51) Keyes, F. *J. Mech. Eng. Sci.* **1931**, *53*, 132–135.

(52) Abdulagatov, I. M. *J. Chem. Thermodyn.* **1997**, *29*, 1387–1407.

(53) Abdulagatov, I. M. *J. Chem. Eng. Data* **1998**, *43*, 830–838.

(54) Gildseth, W. J. *J. Chem. Eng. Data* **1972**, *17*, 402–409.

(55) Osborne, N. S. *J. Res. Nat. Bur. Std.* **1933**, *10*, 155–158.

(56) Douslin, D. R.; Osborn, A. *J. Sci. Instr.* **1965**, *42*, 369.

(57) Egerton, A. *Philos. Trans. R. Soc. Lond. Ser. A* **1932**, *231*, 147.

(58) Besley, L. *J. Chem. Thermodyn.* **1973**, *5*, 397–410.

(59) Jenkin, C. F.; Pye, D. R. *Philos. Trans. R. Soc. Lond. Ser. A* **1914**, *213*, 67.

(60) Sengers, J.; Levelt, H.; Chen, W. T. *J. Chem. Phys.* **1972**, *56*, 595–608.

(61) Meyers, C. H.; van Dusen, M. S. *J. Res. Nat. Bur. Std.* **1933**, *10*, 281.

(62) Webster, L. A.; Kidney, A. J. *J. Chem. Eng. Data* **2001**, *46*, 759–764.

(63) Harris, J. G.; Yung, K. H. *J. Phys. Chem.* **1995**, *99*, 12021–12024.

(64) Nowak, P.; Tielkes, T.; Kleinrham, R.; Wagner, W. *J. Chem. Thermodyn.* **1997**, *29*, 885–889.

(65) Toedheide, K.; Franck, E. U. *Z. Phys. Chem. NF.* **1963**, *37*, 387–401.

(66) Takenouchi, S.; Kennedy, G. C. *Am. J. Sci.* **1964**, 1055–1074.

(67) Archer, A. L.; Amos, M. D.; Jackson, G.; McLure, I. A. *Int. J. Thermophys.* **1996**, *17*, 201–211.

(68) Sultanov, R. G.; Skripka, V. G.; Namiot, A. Y. *Zhurnal Fizicheskoi Khimii* **1972**, *46*, 2160.

(69) Welsch, H. Ph.D. thesis, University of Karlsruhe, 1973.

(70) Brunner, E. *J. Chem. Thermodyn.* **1990**, *22*, 335–353.

(71) Shmonov, V. M.; Sadus, R. J.; Franck, U. *J. Phys. Chem.* **1993**, *97*, 9054–9059.

(72) Smith, B. D.; Srivastava, R. *Physical Science Data: Thermodynamic Data for Pure Componentes, Part A: Hydrocarbons and Ketones. Vol. 25*; Elsevier:; New York, 1986.

(73) Fletcher, D. A.; McMeeking, R. F.; Parkin, D. *J. Chem. Inf. Comput. Sci.* **1996**, *36*, 746–749.

(74) Wei, M. S. W.; Brown, T. S.; Kidnay, A. J.; Sloan, E. D. *J. Chem. Eng. Data* **1995**, *40*, 726–731.

(75) Somait, F. A.; Kidnay, A. J. *J. Chem. Eng. Data* **1978**, *23*, 301–305.

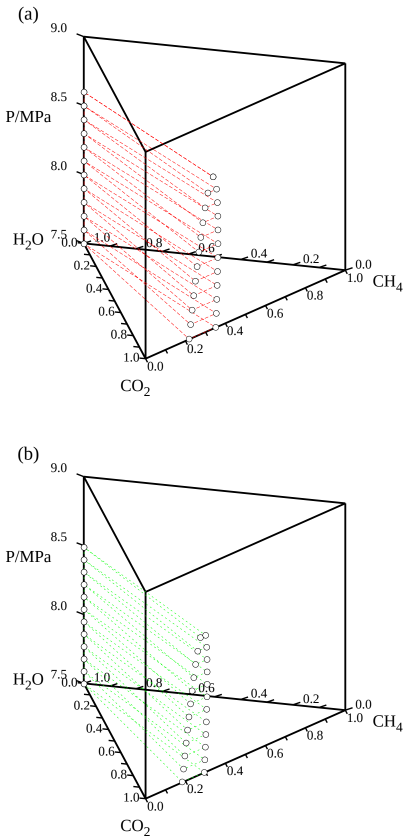

Tridimensional view of the ternary diagram, as a function of pressure, of the mixture $H_2O(1)$ + $CO_2(2)$ + $CH_4(3)$ as predicted from SAFT-VR at low temperatures. The dashed lines represent the sides of the triangles that bound the three-phase LLV coexistence region and the circles their corresponding compositions.